The Interplay of Surface Energy and Depolarizing Field on the Domain Evolution of a Thin-Film Ferroelectric

by

Aulia Tegar Wicaksono

B. Eng, Materials Engineering
Nanyang Technological University, Singapore, 2008

M. Eng, Materials Science and Engineering
Massachusetts Institute of Technology, Cambridge, United States, 2009

SUBMITTED TO THE SMA OFFICE IN PARTIAL
FULFILLMENT OF THE REQUIREMENTS FOR THE DEGREE OF

MASTER OF SCIENCE IN
ADVANCED MATERIALS FOR MICRO- AND NANO-SYSTEM
AT THE SINGAPORE-MIT ALLIANCE

DECEMBER 2009

The Interplay of Surface Energy and Depolarizing Field on the Domain Evolution of a Thin-Film Ferroelectric

by

Aulia Tegar Wicaksono

Submitted to the SMA Office on December 31, 2009

In Partial Fulfillment of the Requirements for the

Degree of Master of Science in

Advanced Materials for Micro- and Nano-Systems

ABSTRACT

The role of depolarizing field and surface energy in the domain evolution of a ferroelectric system is investigated by means of phase-field simulation method using the time-dependent Ginzburg Landau equation. It is found that the presence of depolarizing field in the ferroelectric system can lead to the development of multidomains from the initially uniform-polarization state when the thickness of the ferroelectric decreases below a certain critical value. The increasingly relevant surface energy in thin film ferroelectrics may further aggravate the monodomain stability and contribute to promoting the multidomain state if the gradient polarization across the film thickness becomes increasingly significant. The project aims to study and analyze the individual contribution of both effects as well as the interplay among them. The domain characteristics resulting from the presence of both effects will also be studied and then evaluated using the available theoretical models and experimental results.

Thesis Supervisors:

1. Dr. Nathaniel Ng Kuang Chern, Research Engineer,
   Institute of High Performance Computing (IHPC), A-STAR
2. Prof. Chua Soo Jin (SMA Facilitator), SMA Fellow,
   National University of Singapore (NUS)

Acknowledgments

First and foremost, I wish to express my sincere gratitude to my supervisor, Dr. Nathaniel Ng for his utmost support and guidance. I met Dr. Ng during his talk in NUS on April this year and was particularly interested in knowing more about his work. It was pleasing to know then that he was willing to accept me as his student for the SMA internship program. During this six-month course, I have learnt many things about the field of the project as well as the simulation in general from him. The valuable inputs that he continuously provides have helped me in understanding this fascinating field of research. In addition to that, the immeasurable support in the form of his availability and, more importantly, his suggestions pertaining to my future career are some of the privileges that I have owed him. Because of these reasons, this internship period has been an enriching and memorable experience for me.

I also would like to convey my gratitude to Dr. Rajeev Ahluwalia of IHPC for his feedbacks and suggestions given to me throughout the internship period. His valuable thoughts have helped me in managing the directions of the project. Gratitude is also addressed to Prof. David Srolovitz for his valuable tips and suggestions about the final presentation. I am also thankful to Prof. Chua Soo Jin from SMA for his time and effort spent being my internship facilitator.

My appreciation is also directed to Institute of High Performance Computing (IHPC) for the internship opportunity granted to me, and to Singapore-MIT Alliance for the studentship support during the project. Last, but certainly not the least, I want to deliver my thanks to my parents, my sister and my friends for their paramount and relentless moral support and would personally dedicate this thesis to them.

Table of Contents

List of Figures

List of Tables

Chapter 1
INTRODUCTION

1.1. Background

The switching behavior of ferroelectric nanostructures has attracted significant research interest, particularly in the field of device miniaturization. As the size of ferroelectrics is further scaled into the order of nanometers, several interesting phenomenon begin to appear. Among them are the size effect and the surface effect on the domain switching of the ferroelectric materials. There have been numerous publications reporting the experimental observations of these cases[1],[2]. Several theoretical treatments have consequently been proposed to explain the experimental result[3],[4], while other literatures have attempted to study these phenomena via computer simulation using the available theoretical models[5],[6].

This project aims to provide a profound simulation-based insight to the ferroelectric switching phenomenon in nanostructure. Employing the Devonshire's extension of the Landau-Ginzburg phase transition model in ferroelectric materials[7], Dr. Ng has developed a rigorous and extensive simulation code to study the switching behavior of several ferroelectric materials. A more detailed discussion on the LGD model applied in ferroelectric materials is provided on the subsequent chapter. Using this simulation tool and by applying appropriate conditions (e.g. by initializing the sample structure such that it resembles the piezo-force microscopy and parallel-plate capacitor configuration), Dr. Ng and his colleagues studied the size effect of ferroelectric materials on their switching behavior and discussed the result in his paper published early this year[8].

In this paper, he concluded that the fringing-induced electric field parallel to the surface can result in the nucleation of intermediate 90°-domain. Such effect will be observed on the condition that the thickness exceeds certain critical value h_c since fringing effect would gradually diminish at the thickness lower than h_c. Another size-related effect concerns with the coercive field. As the lateral size of the electrode is reduced, the coercive field—i.e. the field required to switch the domains to zero

polarization—increases and approximates the intrinsic bulk coercive field. This consequently means that thin film ferroelectrics, such as is exhibited by nanostructures, may completely remain unswitched, hence single domain system.

1.2. Objectives

The current project aims to further investigate the switching behavior of ferroelectric nanostructures under the influence of other effect, particularly the surface effect, in addition to the size effect and the depolarizing field. Several theoretical models proposed that the free energy expansion of the LGD model would introduce natural boundary conditions applicable at both surfaces. These boundary conditions would affect the polarization at the surface measurable by a parameter named extrapolation length (λ). A finite extrapolation length would limit the polarization of the ferroelectric system around the surface at a value lower than the spontaneous polarization. The effect of such parameter has been confirmed by several experimental results[9]. In this project, the surface effect on the switching behavior of the ferroelectric is studied.

1.3. Report Organization

Chapter 1 introduces the rationale and the underlying motivation of the project. Chapter 2 describes the fundamental concepts that will be applied in performing the simulation and interpreting the results. Chapter 3 contains sections dedicated to explain some of the assumptions and the methodologies employed in the simulation tool. Chapter 4 discusses and analyzes the simulation results. Chapter 5 summarizes the work on the project.

Chapter 2
LITERATURE REVIEW

On the core of this project is the mean-field theory of phase transition in which the metastable phase of a system is determined from the thermodynamics relationship between the order parameter of the system and the field that governs its development. In other word, the mean-field theory essentially decides which phase is energetically favorable on a given set of conditions. It however does not offer any perspective on the dynamics of the process. The TDGL (time-dependent Ginzburg-Landau) relaxational equation, discussed in Chapter 3, is one that is responsible for developing the kinetics.

2.1. Free Energy of the Ferroelectric System

In discussing the phase transition of a typical ferroelectric system, its total free energy is normally described as a summation of several components—the most significant of which is the Landau free energy. Other form of energy includes electrostatic energy, gradient energy and elastic energy. It is important to note that these forms of energy are actually energy per unit volume, that is, they are defined within the bulk of the system. There is an additional energy term, discussed on the next section, which is applicable within the surface of the system.

2.1.1. Landau Energy

The proposal of Landau and Lifshitz formulated that in order to describe the phase transition in terms of a continuous change in one or more order parameters, the free energy can be expressed as a power series of the order parameter. Such treatment is considered general for any systems exhibiting phase transition phenomenon, such as spinodal decomposition, ferromagnetism, martensitic transformation, etc. Devonshire has applied this formulation to ferroelectrics system with polarization P as the order parameter and the appropriate form of free energy is comprehensively discussed in several classic textbooks such as Ref. [10].

As the Landau energy formulation is essentially derived via Taylor's series expansion of the free energy, its components may be continuously expanded to include higher power terms. Their presence may introduce higher accuracy but signify practically trivial physics. This project follows the acceptable upper limit for power term, i.e. it was capped up to the eight order term which allows for the tilt of the oxygen octahedral.

Further simplification on Devonshire's formulation can be done by considering the crystallography of the system. An extensive but practical guideline to expand and simplify the Landau energy using the crystallographic properties of the ferroelectric material is given in a recent paper by Cao[11]. Applying these principles to the material subject of this study, the cubic $BaTiO_3$, the Landau free energy with two-dimensional order parameter is simplified into:

$$F_{Landau} = \tfrac{1}{2}\alpha_1\left(P_x^2 + P_y^2\right) + \tfrac{1}{4}\alpha_{11}\left(P_x^4 + P_y^4\right) + \tfrac{1}{2}\alpha_{12}\left(P_x P_y\right)^2 + \tfrac{1}{6}\alpha_{111}\left(P_x^6 + P_y^6\right)$$
$$+ \tfrac{1}{2}\alpha_{112}\left(P_x^4 P_y^2 + P_y^4 P_x^2\right) + \tfrac{1}{8}\alpha_{1111}\left(P_x^8 + P_y^8\right) + \tfrac{1}{2}\alpha_{1112}\left(P_x^6 P_y^2 + P_y^6 P_x^2\right) + \tfrac{1}{4}\alpha_{1122}\left(P_x^4 P_y^4\right)$$

The parameter α_1, α_{11}, α_{12}, etc are properties of the material and their values may be determined experimentally or from first principle calculations. The first parameter α_1 is particularly of interest since it dictates the shape of free energy curve around the transition temperature T_c. Due to the ordering nature exhibited at $T < T_c$, this parameter should numerically be negative at this temperature range. And to be consistent with Curie-Weiss law, $\alpha_1 = C(T - T_c)$ and C is the appropriately chosen Curie's constant. To illustrate the significance of this temperature-dependent parameter, the free energy at different temperatures is drawn as a function of the one-dimensional order parameter. When the system is at $T > T_c$, the stable equilibrium is at $P = 0$ (paraelectric state) which corresponds to the positive value of α_1. In the materials under consideration, the transition is of the first-order type and is indicated by $\alpha_{11} < 0$. This type of transition will result in the free energy curve having three minima—$P = \pm P_s$ and $P = 0$—at the transition temperature. At $T < T_c$, the paraelectric state ($P = 0$) is no longer the metastable state, that is, the total energy is not minimized.

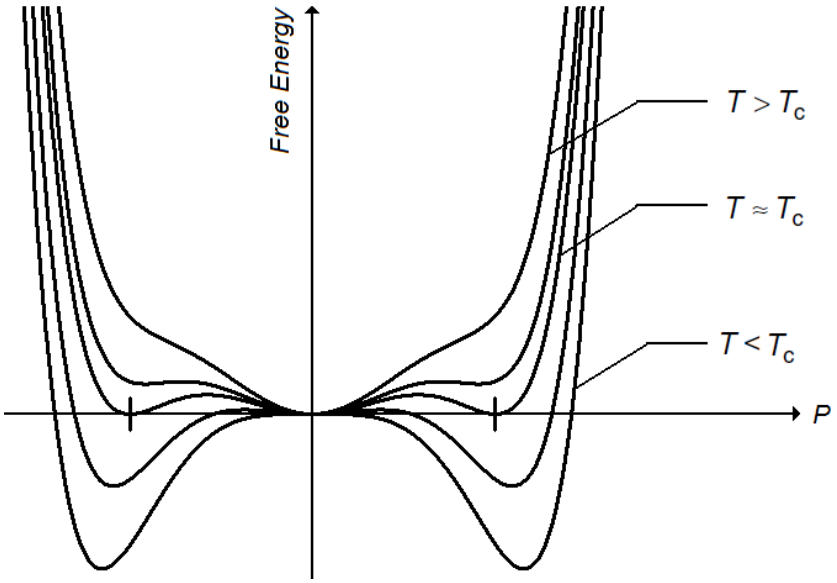

Figure 1 Illustration of free energy as a function of one-dimensional order parameter *P* at different temperatures[12].

2.1.2. Gradient Energy

The presence of domains and domain walls will profoundly affect the macroscopic properties of the ferroelectrics. In order to describe such atomically coherent inhomogeneous structures, one must add energy penalty associated with them. The appropriate term would consist of the gradient of the order parameter and they must also conform to the crystallographic properties of the materials. For the case of $BaTiO_3$, the gradient energy term in two-dimensional order parameter is expressed as:

$$F_{gradient} = \tfrac{1}{2}G_{11}\left(P_{x,x}^2 + P_{y,y}^2\right) + \tfrac{1}{2}G_{12}\left(P_{x,x}P_{y,y}\right) + G_{44}\left(P_{x,y}^2 + P_{x,y}^2\right)$$

The above formulation differs slightly with the one proposed by Nambu and Sagala[13]. Cao argued that the extra term involving the coefficient G_{44}' appeared on Nambu-Sagala's term is not an independent term, hence can be integrated into the G_{12} term[11].

2.1.3. Electrostatic Energy

This energy is associated with electric field developed within the material, including the depolarizing field, and is expressed as:

$$F_{electrostatic} = -[\tfrac{1}{2}\varepsilon_0(E_x^2 + E_y^2) + E_xP_x + E_yP_y]$$

2.1.4. Elastic Energy

Elastic energy plays significant role in explaining the microstructual evolution of a ferroelectric material. This form of energy is derived from the same basis as the Landau energy. Its general form is given as: $F_{elastic} = \frac{1}{2} C_{ijkl} \in_{ij} \in_{kl}$ .Using the same assumptions as one implemented in Landau energy formulation, i.e. cubic crystal system, the elastic energy is written as:

$$F_{elastic} = \tfrac{1}{2} C_{11}\left(\tilde{\in}_{xx}^{2} + \tilde{\in}_{yy}^{2}\right) + C_{12}\left(\tilde{\in}_{xx}\tilde{\in}_{yy}\right) + \tfrac{1}{2} C_{44}\left(\tilde{\in}_{xy}^{2}\right)$$

For an epitaxially grown thin film ferroelectrics with fixed lateral misfit strain (see Section 3.3), the effect of the elastic contribution can be incorporated into simulation by means of rescaling of the coefficients of the Landau free energy.

2.1.5. Surface Energy

The finite size of the ferroelectric introduces the energy term applicable within the surface and is given as:

$$F_{surface} = \tfrac{1}{2} K \lambda^{-1} [P_y^2\big|_{y=0} + P_y^2\big|_{y=h}]$$

Combining both terms as total energy and expressing it in terms of energy per unit area $\overline{F}_{total}$, the full form of the functional thus becomes

$$\overline{F}_{total} = \int_0^h \left(F_{Landau} + F_{grad} + F_{e-static} + F_{elastic}\right) \cdot dy + \tfrac{1}{2} K \lambda^{-1} [P_y^2\big|_{y=0} + P_y^2\big|_{y=h}]$$

2.2. Surface Polarization

Following the Euler-Lagrange formulation, the non-integrand part of the total energy—i.e. the surface energy—essentially provides the natural boundary conditions for such system. While the detailed mathematical treatment is available from Ref. [14], the following describes the important consequence of the surface energy.

$$\left.\frac{dP_y}{dy}\right|_{y=0} - \frac{P_y\big|_{y=0}}{\lambda} = 0 \quad \text{and} \quad \left.\frac{dP_y}{dy}\right|_{y=h} + \frac{P_y\big|_{y=h}}{\lambda} = 0$$

These basically tell about how the behavior of polarization (and polarization gradient) at the surface is affected by the extrapolation length term. Two extreme cases of λ will result in the following:

- The case of $\lambda = 0$:

$$P_y\big|_{y=0} = P_y\big|_{y=h} = 0$$

  In this condition, the lack of long-range ordering at the surface, possibly due to damaged structure, will completely block the polarization at the boundary.

- The case of $\lambda \to \infty$:

$$\left.\frac{dP_y}{dy}\right|_{y=0} = \left.\frac{dP_y}{dy}\right|_{y=h} = 0$$

  This case represents the ideal case in which the surface polarization remains unchanged with respect to the bulk polarization.

These two extremum of λ may be interpreted as the upper and lower bound of the extrapolation length of a typical real ferroelectric system. However, we also note that there have been several theoretical models proposing the existence of negative extrapolation length[15]. In such hypothetical system, the surface polarization is higher than the bulk polarization which theoretically leads into higher transition temperature and requires a different physical model to explain. Another theoretical proposal is concerning a system with asymmetric extrapolation length. Such can occur if different surface treatment (morphology, chemical bonding, mechanical clamping, etc) applies for the top and bottom surface. In this project, only symmetric positive extrapolation length is treated—the above two proposals are not addressed.

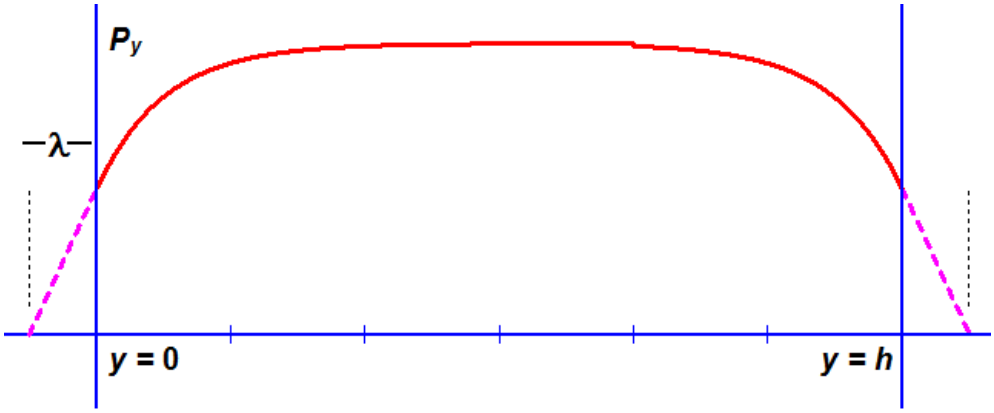

Figure 2 Illustration of the polarization along the thickness of the sample and how the extrapolation length is measured accordingly

Physical interpretation of λ

The extrapolation length λ, which according to experimental reports[9] ranges from 0.5 to 50 nm, may initially appear as a mere mathematical tool arising as a consequence of yet another mathematical formulation. The physics on ferroelectricity can however offer a more insightful meaning of it. The physical interpretation starts from the surface energy term. In its general form, the surface energy is written as $F_{surf} = \int \gamma \cdot dA$ where γ is the surface tension coefficient. A small finite change in area dA can be expressed in terms of the strain element. In this case, only strain oriented parallel to the surface is considered, that is, $dA = (\in_{xx} + \in_{zz})dx \cdot dz$

Considering no external force acting on the element, the aforementioned strain is induced by polarization via the electrostrictive effect. Substitution of each of these relations, the surface energy term is now $F_{surf} = \int \gamma (q_{12}P_y^2 + q_{32}P_y^2) \cdot dx \cdot dz$ where q_{ij} is the electrostrictive tensor coefficient written in shortened form (i.e. Voigt notation). Comparing this energy form with one formulated in Section 2.1.5, the extrapolation length may be expressed as $\lambda = \frac{K}{2\gamma q_{ij}}$ [16]. The above definition of λ shows that it has temperature-dependent characteristics as $\gamma = \gamma(T)$. Furthermore, the definition shows that the sign of extrapolation length will follow that of the gradient coefficient K since surface tension is a positive-definite parameter[17].

2.3. Depolarizing field

The depolarization field is produced by bound charges existing at the polar surfaces of the sample and at the charged walls of the domains encountering in the bulk ("head to head" or "tail to tail"). The surface charge density for the ferroelectric plate cut perpendicular to the polar axis is equal to spontaneous polarization. For typical ferroelectrics the depolarization field strength in a single-domain state can reach the value of 10^8 V/m[18] . This enormous field can be reduced by the formation of 180° striped domain structures.

The presence of uncompensated bound charges gives rise to the depolarization field, or in terms of mathematical relations,

$$\rho_{bound} = -\nabla \cdot P$$

This charge density term has a potentially important role in determining the total electric field that occurs in the ferroelectric material which is formulated as:

$$E(z) = E_{real}(z) + E_{dep}(z) + E_{ext}$$

where each component is described as follows:

- $E_{real}(z) = \frac{1}{\varepsilon_0}\int \rho_{real}(z) \cdot dz$
- $E_{dep}(z) = \frac{1}{\varepsilon_0}\int \rho_{bound}(z) \cdot dz$
- $E_{ext} = \frac{V_{ext}}{L}$

The actual analytical form of depolarizing field would require solving the above equation.

Chapter 3
THE TDGL SIMULATION CODE

3.1. Main Components

The TDGL model, when coupled with electrostatic and elastic effects, can be used to simulate microstructral evolution in ferroelectrics consistent with experimental observations. Electrostatic effects are incorporated through an electrostatic term in the free energy and require the Maxwell equation, Gauss's Law, to be solved at every time step. Elastic effects are incorporated through the elastic free energy term in the free energy.

3.1.1. The TDGL Equation

The simulation of ferroelectric switching behavior is performed using the phase-field method. In this method, the kinetics of domain evolution is governed by the time-dependent Ginzburg-Landau (TDGL) relaxation equation (also known as Allen-Cahn equation or Landau-Khalatnikov equation), i.e.

$$\frac{\partial P_i}{\partial t} = -\Gamma \frac{\delta F_{total}}{\delta P_i}$$

The TDGL equation essentially dictates how the order parameter in a system—in this case, the polarization *P*—would evolve in space-time domain. A complete form of TDGL would comprise subscript *i* that consists of three mutually orthogonal spatial axes (*x*, *y* and *z*). In a two-dimensional model, only two spatial axes are represented. The sign δ denotes the functional derivative and Γ is the coefficient associated with domain wall motion.

In the earlier literatures on the kinetics of microstructure evolution, the TDGL kinetic equation was typically solved using Fourier transform[19]. This requires conversion of the real space into *k*-space (reciprocal space) and its reversal back into real space upon

the completion of computation. The model in this study, however, uses a purely real-space approach, which does not require conversion from real to *k*-space and back.

3.1.2. Gauss' Law for Electricity

The electricity version of Gauss' law needs to be solved in order to obtain the electric potential distribution $\phi(x, y)$ which will in turn be needed to solve the TDGL equation. The analytical form of $\phi(x, y)$ is obtained as the solution of the following equation.

$$\nabla \cdot \mathbf{D} = \rho_{\text{real}} \quad \Rightarrow \quad \nabla \cdot (\varepsilon_0 \mathbf{E} + \mathbf{P}) = \rho_{\text{real}}$$

$$\varepsilon_0 \nabla \cdot \mathbf{E} + \nabla \cdot \mathbf{P} = \rho_{\text{real}}$$

$$\varepsilon_0 \nabla \cdot (-\nabla \phi) - \rho_{\text{bound}} = \rho_{\text{real}}$$

$$-\varepsilon_0 \nabla^2 \phi - \rho_{\text{bound}} = \rho_{\text{real}}$$

$$\nabla^2 \phi = -\frac{\rho_{\text{bound}} + \rho_{\text{real}}}{\varepsilon_0}$$

Similar to the case of solving TDGL equation, the solution of the above equation is also approached using the finite difference method. An important point from the above formulation concerns with how the charge density is defined. In this equation, one can choose to consider the effect of depolarizing field by setting the bound charge density ρ_{bound} according to the definition given earlier (or vice versa by setting $\rho_{\text{bound}} = 0$). For simplicity's sake, the real charge density can also be set to zero such is implemented in this project.

3.1.3. Combining the main components

Domain evolution is simulated using the TDGL equations, with the electrostatic energy term as described in section (2.1.3) included into the total free energy, with the value of ϕ obtained by solving Gauss's Law at every time step. In order to provide a much clearer perspective, an intermediate summary of the simulation program is presented. There are two sets of equation systems that must be solved in order to understand the kinetics of domain evolution of the ferroelectric system. Each of them is solved iteratively as the time parameter progresses and is shown in the following illustration.

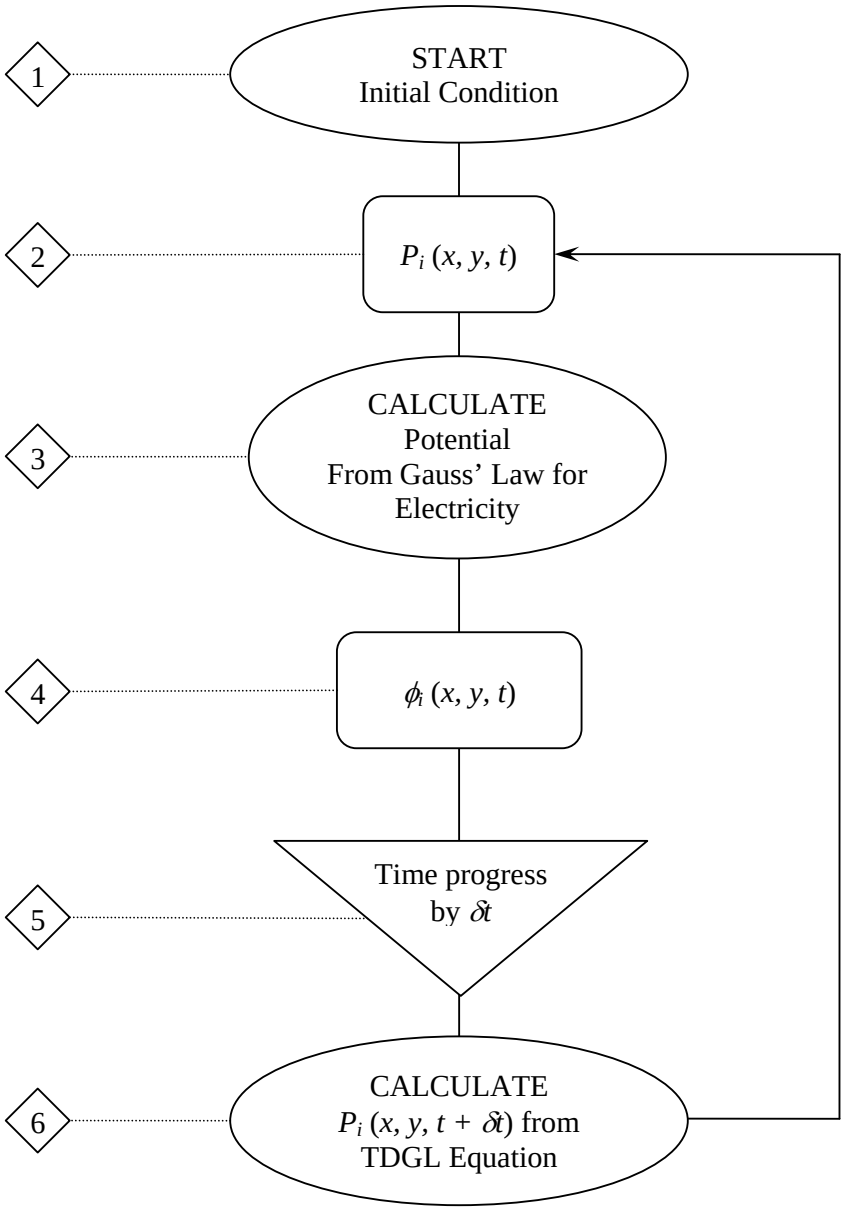

Figure 3 Diagram flow of the iterative computation loop in the simulation program

3.2. Supporting Components

In addition to the core building blocks discussed earlier, several supporting components are integrated into the program. It is to be noted that these components are labeled as "supporting" due to the fact that without their presence the main

components can still perform its fundamental function of simulating the phase field microstructural evolution. The addition of a supporting component such as the Maxwell solver allows us to observe the role of the Maxwell equation in the behavior of the material. Detailed discussion about them is presented in this section.

3.2.1. Rescaled parameters

The physical parameters are rescaled to ensure that the risk of computational error that arises due to the truncation is kept to a minimum degree. For each parameter, the corresponding rescaled parameter can be obtained by normalizing the parameter with some standard value of that parameter that may be chosen arbitrarily or using some characteristic value. For example, the rescaled polarization is obtained by normalizing the polarization with the spontaneous polarization P_S. Such normalization scheme proves to be practically useful, i.e. it offers the flexibility in implementing different set of material parameters. In this project, discussion concerning any physical parameters has implicitly incorporated the rescaled parameters whose complete list is in Table 1.

Table 1 List of the rescaled parameters and their scaling factor

Parameters	Rescaled parameters
Polarization	$P' = P / P_s$ where P_S is spontaneous polarization
Length	$l' = \frac{l}{\delta}$ where δ is chosen as 1 nm
Electric field	$E' = E / E_0 = \frac{E}{P_S / \varepsilon_0}$ where ε_0 is the vacuum permittivity
Voltage	$\phi' = \phi / \phi_0 = \frac{\phi}{P_S \delta / \varepsilon_0}$
Strain	$\in' = \in / \in_0 = \frac{\in}{Q_{11} P_S^2}$ where Q_{11} is the appropriately chosen electrostrictive coefficient.
Stress	$\sigma' = \sigma / \sigma_0 = \frac{\sigma}{C_{11} Q_{11} P_S^2}$ where C_{11} is the appropriately chosen elastic coefficient.

Landau coefficient	$\alpha_n' = \frac{\alpha_n}{\lvert \alpha_1 \rvert / P_S^{2(n-1)}}$ where n is the rank of the tensor
Gradient coefficient	$G_n' = \frac{G_n}{\delta^2 \lvert \alpha_1 \rvert}$

3.2.2. The boundary condition formulation

The surface effect is introduced into the existing TDGL code by translating the boundary condition with extrapolation length into its discretized form. Proper care, however, must be exercised in doing so since errors such as division by zero might arise from a poor formulation. The approach taken for the boundary condition is expressed as follows. Here, the formulation for one of the polarization component (P_y) at the top surface is discussed. Note the simplicity that it offers as compared to those described in Ref [20].

$$\frac{P_y(j=2) - P_y(j=0)}{2\delta} = \frac{P_y(j=0)}{\lambda_{top}} \Leftrightarrow P_y(j=0) = \frac{\lambda_{top}}{2+\lambda_{top}} P_y(j=2)$$

where δ is the scaling factor for the reduced length (δ = 1 nm).

In addition to that, the double-padding scheme as implemented in the earlier works and illustrated in Figure 4 will also be applied here. In such case, another boundary condition is established for the midpoint of the double-pad, that is.

$$P_y(j=1) = \tfrac{1}{2}\left(P_y(j=0) + P_y(j=2)\right)$$

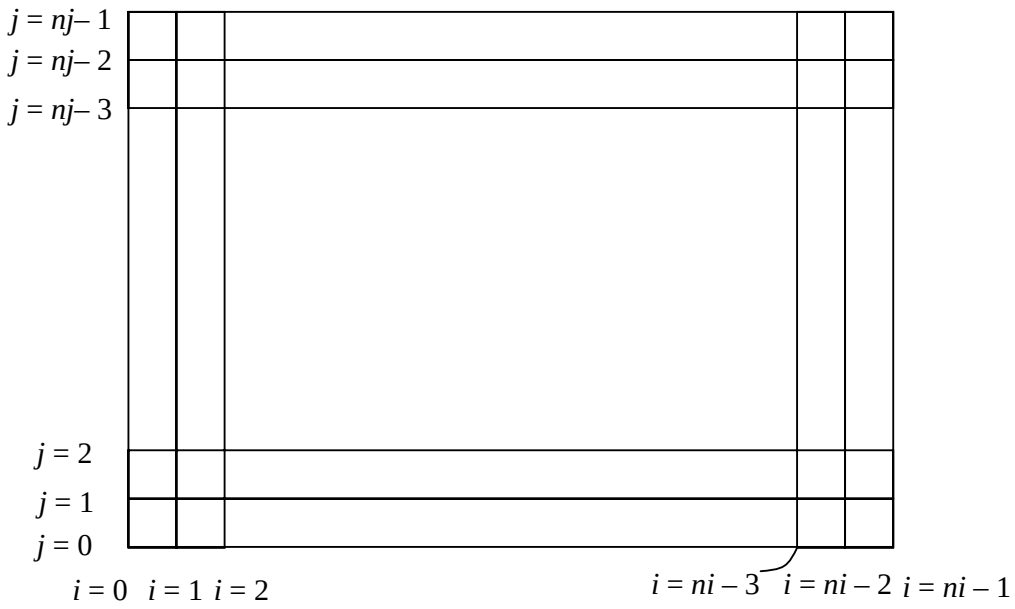

Figure 4 Double-pad scheme for discretizing the boundary conditions

3.2.3. Gaussian noise

Most classical studies on the phase evolution of ferroelectrics employ deterministic approach in which the parameters involved can be determined directly from analytical expressions—some examples of which are given on Ref. [3] and [4]. Such treatment are in complete opposite with the increasingly developing research field in which the *ab-initio* methods with stochastic nature such as DFT and Hartree-Fock calculations are employed to understand the behavior of ferroelectrics—an example of which is available from Ref. [21].

The approach implemented in this project essentially leans towards the deterministic approach with one stochastic component, that is, the Gaussian thermal noise. The randomly distributed small deviation is introduced to the two possible initial conditions: the uniaxially polarized (mean P/P_s of 1.0 and standard deviation of 0.001) and the paraelectric state (mean of 0.0 and standard deviation of 0.001). This Gaussian noise is added to ensure that any development observed during the simulation does not occur due to numerical artifacts.

3.3. Parameter and Simulation Condition

The simulation will use $BaTiO_3$, an extensively studied perovskite ferroelectric material, under room temperature as the subject. More particularly, the condition employed by Pertsev et al[22] will be adapted in which a thin film of barium titanate is epitaxially deposited on a substrate such that a uniform lateral strain of $\in_0 = -0.022$ is introduced. The parameters of barium titanate that correspond to this particular condition are listed in the following table.

Table 2 Material properties of strained-$BaTiO_3$[5][22]

Spontaneous Polarization	P_s	3.429350×10^{-1} C·m^{-2}		C_{11}	1.780×10^{11} N/m^2
Landau Energy Coefficients	α_1	-7.54692×10^7 m/F	Elastic coefficient	C_{12}	0.964×10^{11} N/m^2
	α_{11}	-2.097×10^7 m^5/C^{2}F		C_{44}	1.220×10^{11} N/m^2
	α_{12}	7.97400×10^8 m^5/C^{2}F	Electrostrictive coefficient	Q_{11}	0.100 m^4/C^2
	α_{111}	1.294000×10^9 m^9/C^{4}F		Q_{12}	-0.045 m^4/C^2
	α_{112}	-1.950000×10^9 m^9/C^{4}F		Q_{44}	0.059 m^4/C^2
	α_{123}	-2.500000×10^9 m^9/C^{4}F	Gradient term	G_{11}	6.08518×10^{-10} J m^3/C^2
	α_{1111}	3.863000×10^{10} m^{13}/C^{6}F			
	α_{1112}	2.529000×10^{10} m^{13}/C^{6}F			
	α_{1122}	1.637000×10^{10} m^{13}/C^{6}F			

There are two set of dimensions that will be used as the simulation standard: the $64 \times h$ sample and the $128 \times h$ sample. The former will be used to investigate the effect of surface energy and depolarizing field on the monodomain stability while the latter is employed to study the multi-domain characteristics. In each scenario, the sample

thickness will be varied to observe the size effect on some of the parameters from the simulation.

In order to allow sufficient development of the domain structure, most of the simulation works will be performed up to 500,000 time steps. Some of them may be terminated earlier if the domain morphology exhibits no change after 20,000 time steps but each of them is simulated for at least 50,000 time steps.

Chapter 4
RESULTS AND DISCUSSIONS

This chapter will commence with the discussion about the effect of surface energy term and the depolarizing field on the monodomain stability. After the individual effect of these conditions is identified, the discussion will proceed to the simulation results in which both effects are present. Using these results, the domain pattern and characteristics will be analyzed and compared with the available theoretical model and empirical results reported on several literatures.

4.1. Simulation Outline

4.1.1. Monodomain stability

Levanyuk et al[23] concluded that the presence of depolarizing field will drive an initially monodomain ferroelectrics to assume the multidomain state. In order to observe the extent to which the depolarizing field will affect the monodomain stability, the simulation will start by considering a system in which the contribution of the electrostatic energy to the total energy is removed. The surface energy term, nevertheless, still remains as indicated by the finite extrapolation length parameter. In the simulation code, this condition is simulated by excluding the Gauss' Law solver from the computing blocks in Figure 3.

The average and maximum polarization, denoted as $<P>$ and $|P|_{max}$ and obtained from this condition, are particularly of interest since they reflect the system's resilience in sustaining the initially uniformly-polarized state under the presence of surface energy. Sample thickness will act as the independent variable against which the dependent variables of average and maximum polarization will be plotted.

In order to provide a more complete understanding on the monodomain stability, the extent to which the surface energy affects the domain splitting will be explored by varying the magnitude of extrapolation length. There are three values of extrapolation length under consideration: 2, 50 and 100. They are chosen so as to represent different

surface conditions as explained in Section 2.2—small λ indicates intensive reduction of surface polarization possibly caused by degraded, damaged or reconstructed surface while large λ indicates smaller contribution of surface energy and further implies a near-perfect surface condition.

After the surface energy effect has been investigated using the above plan, the effect of depolarizing field is then reintroduced by including the Gauss' Law solver into the computation blocks. In doing so, the project will employ two cases: firstly, the depolarizing field that is applicable throughout the film and secondly, the depolarizing field that is applicable only within the bulk but not at the surface. The former case closely resembles the condition found in most of ferroelectric with open and/or untreated surface—i.e. no contact with other materials—while the latter corresponds to a ferroelectric system in which the surface bound charge has been compensated, i.e. $\rho = \nabla \cdot P$, by means of interface with metal electrodes and other methods[24].

4.1.2. Domain pattern and characteristics

The subsequent simulation aims to investigate the domain pattern from an initially monodomain ferroelectric. The case of depolarizing field applicable at both surface and bulk will be assumed. The setup in this case is as follows. Three values extrapolation length will be used i.e. 1, 10 and 20. They are chosen so as to mimic the experimentally verified values, that is, between 0.5 to 50 nm. The simulation lateral width still follows the convention mentioned earlier, i.e. w = 128, and the film thickness for each λ starts with 16 and will vary according to its respective critical thickness h_c as obtained from the previous simulation outline.

The simulation with the paraelectric initial state simulates a ferroelectric quenched from a temperature above T_c to the room temperature. This result is compared to the simulation which starts from an initial monodomain state—if the results differ, it means that in one of these scenarios, the system is trapped in a metastable state. We also note that in the case of paraelectric initial condition, no critical thickness h_c is observed as the system goes into a multidomain state in all cases and does not enter into a monodomain state. This is consistent with the observation by Levanyuk et al[23]

who concluded that the monodomain state is always metastable in the presence of a depolarizing field.

4.2. Discussions

4.2.1. Monodomain stability

This section will start with the discussion of the effect of three different scenarios outlined in Section 4.1.1 on the average polarization and maximum polarization, i.e. (1) exclusion of the electric field contribution, (2) contribution of depolarizing field but with charge compensation at the surface (i.e. $\rho = \nabla \cdot P$) (3) no charge compensation at all (depolarizing field applicable throughout the sample).

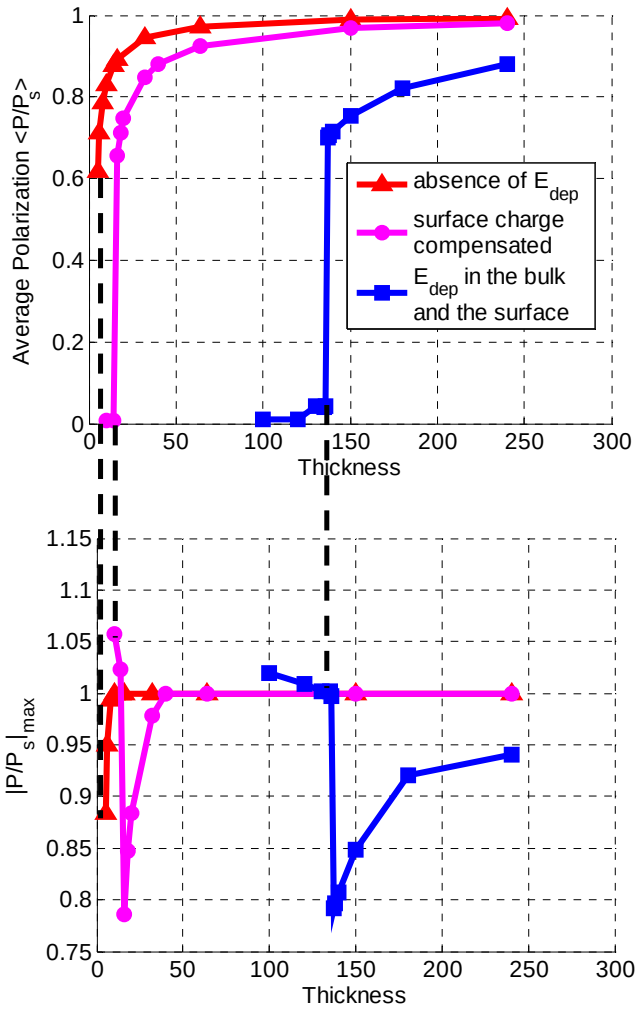

Figure 5 (a) Average and (b) maximum polarization as a function of thickness for $\lambda = 2.0$.

The absence of depolarizing field (scenario 1) allows the monodomain ferroelectrics to remain metastable even at extremely low thickness. We also note that due to the double-pad scheme (Section 3.2.2) which requires four points to define, simulation with sample thickness below $h = 5$ cannot be tested.

In scenario 3, the presence of the depolarizing field would promote the formation of the multidomain state when the film thickness decreases beyond the threshold h_c— whose value is 136 in the case of $\lambda = 2.0$. As the thickness further decreases, the depolarizing field E_{dep} becomes significant so that in order to reduce the energy cost associated with large E_{dep} in thinner films, formation of multidomain is energetically preferred. The following illustration is presented to demonstrate how the multidomain structure can lower the total energy.

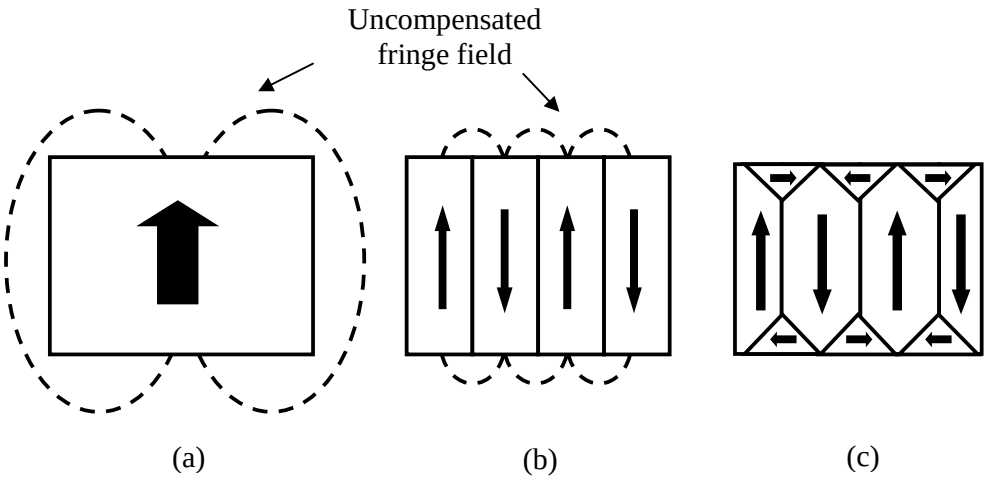

Figure 6 Illustration of ferroelectric domains in
(a) monodomain, (b) 180°-domain structure and (c) 90°-domain structure

The presence of the depolarizing field in the case of monodomain creates uncompensated fringe electric field near the surface. Such field contributes to the electrostatic energy and can be reduced by the formation of 180°-domain structure in which domains of opposite orientation are adjacent to each other. The fringe field, nevertheless, still prevails in this structure albeit its magnitude has been appreciably reduced. Further compensation of fringe field may occur when the attempt on rotating the domain orientation does not lead to significant increase in the total energy. In such case, a 90°-domain structure may develop as shown in Figure 6c.

To further verify the formation of such structure, the sequence of domain evolution as generated by the simulation code is presented in the following figures which have been extracted from the 64×120 sample. The 'green' domain represents the up-polarization (P_y/P_s = +1.0) while the 'purple' represents P_y/P_s = –1.0. This chronological sequence shows that the 90°-domain structure has indeed developed near the surface as indicated by the small 'red', i.e. P_x/P_s = +1.0 and 'white', i.e. P_x/P_s = –1.0 domains representing polarization at lateral direction.

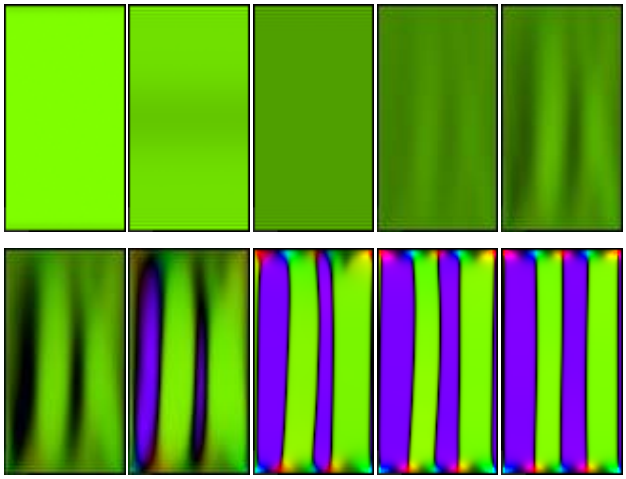

Figure 7 Domain evolution in 64×120 sample with λ = 2.0

As the thickness of the simulation sample approaches the critical thickness in Figure 5, and yet is still in the initial monodomain state, the polarization anywhere within the system is diminishing due to the presence of increasing E_{dep}. The average polarization $<P>$ and the maximum polarization $|P|_{max}$ will consequently decrease as reflected in Figure 5a and b. When multidomain state is finally reached, the average polarization drops significantly due to the presence of the recently developed down-domain illustrated in Figure 7 while the maximum polarization is no longer limited to its initial spontaneous polarization—that is, $|P|_{max} > P_s$.

The case of surface charge compensation (scenario 2) as demonstrated by the middle plot of Figure 5a and b is particularly of interest. Such scenario is proposed to help maintaining the stability of monodomain state at an even lower thickness ($h < h_c$) despite the presence of E_{dep} in the bulk. The simulation results nevertheless show that

even though the proposal does indeed result in a smaller h_c, the formation of multidomain can still occur as illustrated in the sudden drop of average polarization.

This indication of multidomain formation is no longer attributed to the presence of depolarizing field in the bulk but due to the fact that the polarization gradient along the film surface (i.e. $y = 0$ and $y = h$) is relatively large for this set of simulation parameter ($\lambda = 2.0$). Figure 8 shows the magnitude comparison of the polarization gradient for each value of λ. The energy cost associated by this gradient can be accommodated in many ways; one of which is via the multidomain formation.

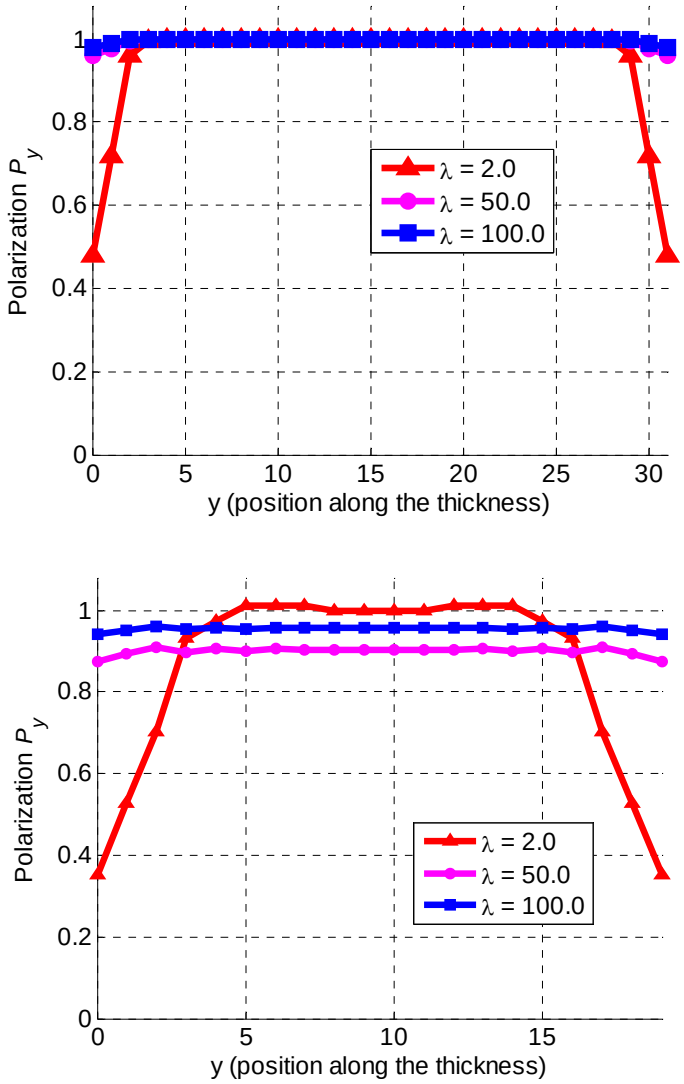

Figure 8 Polarization profile across the film thickness under (top) the absence, or Scenario 2 and (bottom) the presence of depolarizing field, or Scenario 3, at the film surface

To illustrate the extent to which the surface energy affects the monodomain stability, the following plot depicts the average polarization as a function of thickness for different values of extrapolation length under the condition of surface charge compensation.

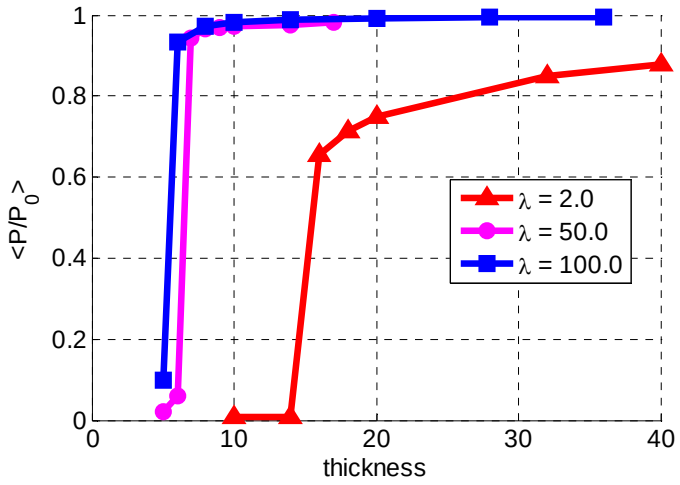

Figure 9 Average polarization vs thickness under the condition of surface charge compensation

Figure 9 above shows that at larger extrapolation lengths (i.e. λ = 50.0, 100.0), their critical thickness is almost identical and it approaches the critical thickness corresponding to the case in which the depolarizing field is absent (h_c = 5). It can thus be concluded that the charge compensation at the surface indeed does help in maintaining the stability of monodomain state. Such is however only applicable under the condition in which the surface energy term is sufficiently small that the polarization gradient across the film thickness would not generate additional energy contributions which encourages the multidomain formation. The set of simulation with λ = 2.0 certainly does not satisfy this condition as shown in the polarization profile of Figure 8.

4.2.2. Critical thickness

The subsequent discussion on the simulation results would employ the condition in which no charge compensation occurs anywhere in the system, that is, the depolarizing field is present both within the bulk and at the surface. This condition can be regarded

as the least preferred scenario and affects the monodomain stability the most among the three scenarios discussed earlier.

It is previously understood that under this condition, there exists a critical thickness beyond which the monodomain state would split into multidomains. It is of interest to establish the relationship between the magnitude of the extrapolation length with the critical thickness to which it is associated.

In doing so, the simulation is performed for a 128×*h* sample. The dimension *h* would be varied to determine h_c. After h_c for a given λ has been identified, similar simulation is then performed on four different samples whose lateral width is an integer multiple of the original lateral width (256, 384, 512 and 640 nm).

The motivation for doing the copious measurements is to achieve statistically reliable data. This is so since the initial random noise may slightly affect the critical thickness of a particular extrapolation length under different lateral widths even though the lateral width is itself an independent parameter, i.e. whose magnitude has no effect on the measured parameter, The following plot shows the critical thickness for different value of λ—whose detailed list is available at Appendix—along with the vertical error bar, which is too small to be visible in the plot.

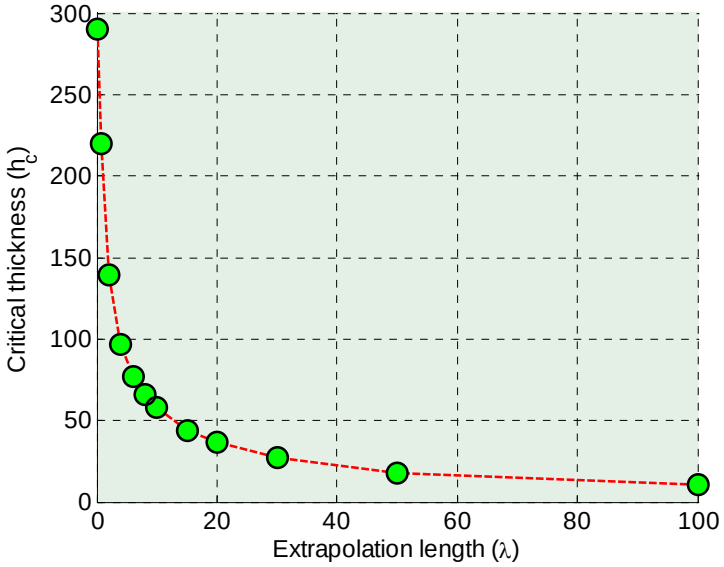

Figure 10 Critical thickness as plotted against the extrapolation length

The relationship displayed in Figure 10 above further emphasizes the significant role of surface energy in the monodomain stability while the asymptotic trend may potentially originate from the reciprocal relationship between the surface energy and the extrapolation length.

4.2.3. Average domain width

The discussion now continues with the study of the domain pattern and its characteristics when multidomain state develops. In doing so, the simulation will start by verifying the influence, if any, of two different initial conditions on the domain patterns and size. The two sequences presented in the following figures are extracted from the 128×40 sample with $\lambda = 2.0$ to verify that the different initial condition does not lead to different domain pattern and characteristics.

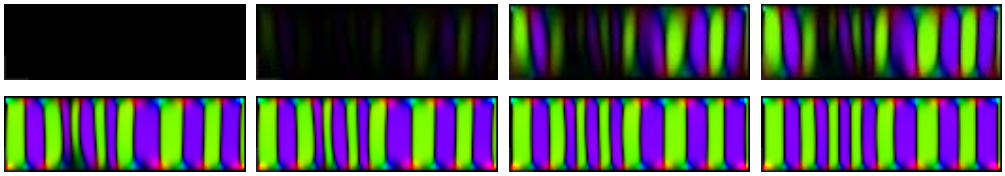

Figure 11 Domain evolution in 128×40 sample with $\lambda = 2.0$ and paraelectric initial state

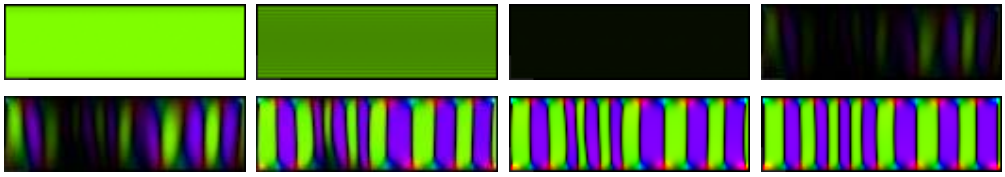

Figure 12 Domain sequence in 128×40 sample with $\lambda = 2.0$ and monodomain initial state

When the monodomain state is used as the initial condition of the ferroelectric system, the valid thickness interval for observing the domain pattern is restricted by the critical thickness h_c. Table 3 details the thickness that will be used for different values of λ

Table 3 List of the sample thickness chosen for the study of domain pattern

λ	h_c	Sample thickness					
1.0	> 140	16	32	48	64	80	96
10.0	66	16	24	32	40	48	64
20.0	37	16	20	24	28	32	36

Although it was already shown that the monodomain and paraelectric initial state does not lead to different domain patterns, the simulation using the latter initial state is still performed so as to show that in both cases, the system does not get trapped in any intermediate metastable state and that the final state is likely to be the stable state that minimizes the total energy.

Similar to the case of critical thickness measurement in Section 4.2.2, the lateral width that spans in the same interval (128 – 640 nm) will also be used as the statistic control parameter.

The following set of figures illustrates the final state of the sample with paraelectric initial state after developing into multi-domains. Here, the snapshots from the lateral width of 384 nm and thickness of 32, 64 and 96 nm are shown. The same set of snapshots from three value of extrapolation lengths are juxtaposed against each other for comparison purposes. From these snapshots, one can easily identify the underlying qualitative trends of the average domain width for varying conditions: the domain width expands as the sample thickens and the extrapolation length increases.

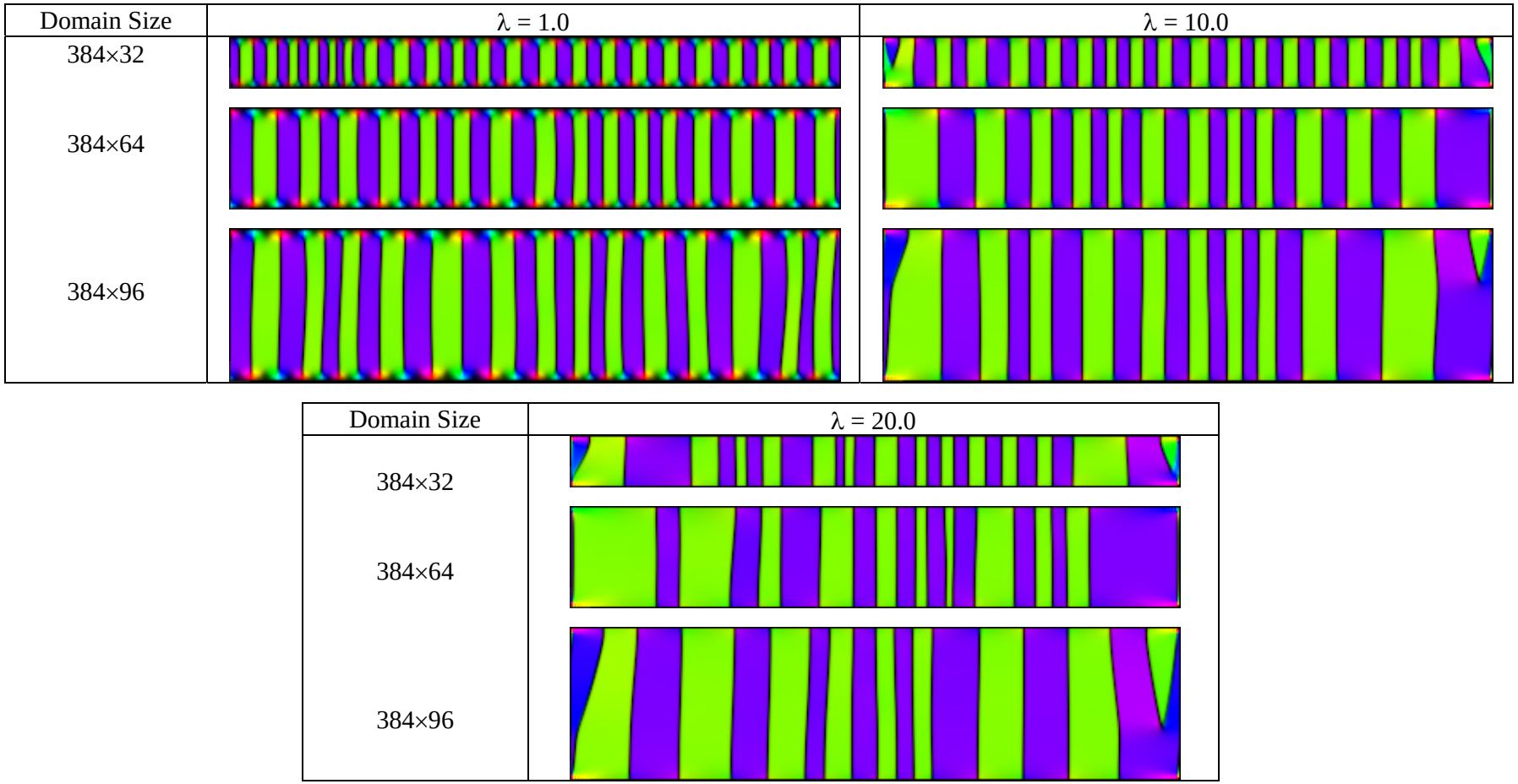

Figure 13 Final morphology of the ferroelectric sample under different extrapolation lengths and different sample thickness

In order to interpret the trend and provide a more meaningful discussion, the average domain width for each simulation results is calculated. When doing so, one should be reminded of the following fact: the sample exhibits a periodic boundary condition. Therefore, by symmetry, the number of domains is restricted to even numbers. Hence, the observed widths may not be accurate due to the potentially high errors.

To appreciate the relationship of average domain width with the sample thickness, this report refers to earlier papers on ferromagnetic domain, particularly by Kittel and other authors[25],[26]. They presented theoretical argument via deterministic assumptions (and neglecting the stochastic nature of dynamic evolution) that the thickness dependence of the domain width should follow the relation of $\overline{w}_d = kh^{1/2}$ (where k is a constant)[27]. Using the data obtained from the simulation, the average domain width against the square root of sample thickness is drawn in three plots, each representing different value of lambda. It can be seen that the relationship established from these data is qualitatively in accordance with the theoretical concept proposed earlier. The agreement in terms of the order of magnitude with the experimental report is also observed using the data available from Ref. [28].

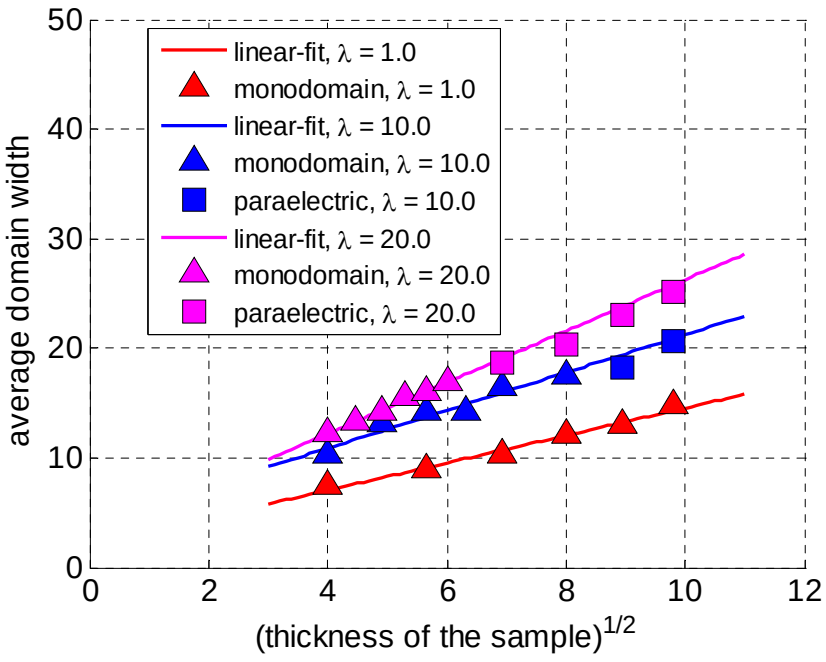

Figure 14 The average domain width vs. square root sample thickness for different extrapolation lengths

Another appealing trend observed from this plot is that the gradient of each line becomes steeper as the extrapolation length that it represents increases. Additionally, the small slope change might indicate the logarithmic dependence of the extrapolation length to the average domain width. It might be of interest to compare the plot from the simulation with the one obtained from the experimental work using Rochelle salt ($KNaC_4H_4O_6 \cdot 4H_2O$) and $PbTiO_3$ as is shown below.

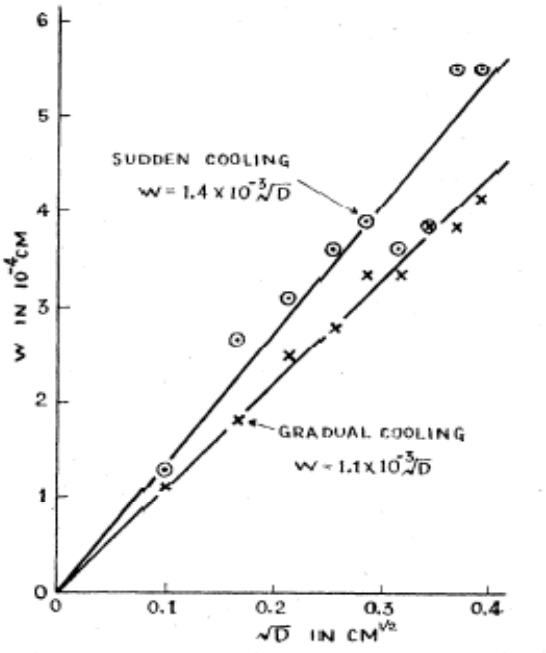

Figure 15 Domain width vs sample thickness of Rochelle salt as measured experimentally[25]

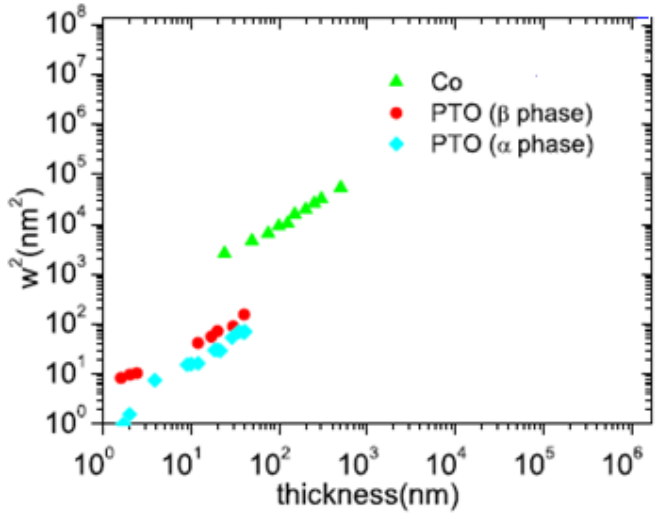

Figure 16 Domain width vs sample thickness of PTO sample[29]

A plausibly speculative conclusion can be drawn from the comparison of both plots. For a given sample size, the average domain width of the suddenly-cooled sample is larger than that of the gradually cooled sample. Thermally-driven diffusion alone is insufficient, or even contradictory, to explain such trend—additional surface-related phenomenon is thought to contribute to this phenomenon. In a suddenly-cooled sample, the kinetics allows very limited time for the surface rearrangement (e.g. surface reconstruction or relaxation) to occur, making the polarization less likely to be abruptly terminated at the surface by the crystalline discontinuity which further leads to an apparently large extrapolation length. The opposite case occurs if the sample is gradually cooled, allowing sufficient time for surface-polarization to develop and resulting in lower extrapolation length.

Chapter 5
CONCLUSIONS

The TDGL simulation code developed by Dr. Ng and his colleagues has proven to be a versatile and insightful tool to understand the thin-film ferroelectric domain evolution via the phenomenological theory. In this project, the switching behavior under the effect of surface energy and the depolarizing field is investigated.

5.1. Individual Effect of Surface Energy and Depolarizing Field

Using the materials and the physical assumptions discussed in Chapter 3, the simulation started with the observation of the monodomain stability under the absence of depolarizing field throughout the system. It is concluded that the monodomain state remains stable regardless of the extent of the surface energy term. On the opposite scenario in which the depolarizing field prevails within the bulk and at the surface, an initially monodomain ferroelectric film may evolve into a multidomain state if its thickness is further lowered below its critical value. The splitting into multidomain process is driven by energy considerations—i.e. to compensate for the energy cost due to the contribution of electrostatic energy.

One of the possible ways to improve the ferroelectric materials' resilience towards depolarizing field is to compensate for the bound-charge at the surface by means of, for example, contact with metal electrode[24]. It was shown that such strategy does indeed lead to the better monodomain stability, that is, the critical thickness reduces appreciably from its value associated with the condition in which there is no charge compensation at the surface.

This strategy, nevertheless, would only work under the condition that the surface energy term of the ferroelectric system is sufficiently small (or the extrapolation length is large) that the polarization at the surface does not differ much with the polarization at the bulk. If their difference—i.e. the polarization gradient—is too significant, additional energy term associated with this polarization gradient will contribute the

total energy. This would consequently drive the formation of multidomain state despite having the bound-charge compensated at the surface.

5.2 Combined Effect

The presence of both surface energy and depolarizing field throughout the system is considered as the least preferred situation, hence indicating the 'worst' scenario, for maintaining the monodomain stability. The monodomain will split into multidomains as the thickness decreases beyond certain value h_c. Carrying out this assumption throughout the rest of the project, the domain pattern and characteristics of the multidomain state are studied and analyzed.

First, the relationship between the extrapolation length with its corresponding critical thickness is established for a considerably wide range of λ. The set of simulation sample thicknesses to study the domain pattern under a given λ are then determined by using the limitation imposed by the previous result (h_c vs. λ). Additionally, a different type of initial condition—the paraelectric state—is also incorporated into the simulation to verify that the initial state of the ferroelectric has little, or in this case no, effect in determining the final domain structure. And by using lateral width as a statistical control parameter, the simulation to study the average domain width is then carried out.

There are two dependent simulation parameters governing the domain morphology: the thickness of the sample and the extrapolation length. The simulation results then conclude that the average width of the domain grows bigger as the sample thickens and as the extrapolation length increases. Furthermore, the qualitative trend of the calculated average domain width indicates a good agreement with the theoretical proposal by Kittel and various reported experimental results[25 – 28].

Appendix

NUMERICAL DATA

Plot 1: Critical thickness (Figure 10)

λ	Critical thickness h_c					Average	STD*
	128	256	384	512	640		
0.1	290	289	291	290	291	290	1
0.667	220	218	222	220	221	220	1
2.0	138	140	138	139	142	139	2
4.0	96	97	96	98	96	97	1
6.0	77	78	76	78	77	77	1
8.0	66	65	66	67	68	66	1
10.0	57	58	58	59	58	58	1
15.0	44	43	44	45	44	44	1
20.0	37	38	37	37	38	37	0
30.0	27	28	26	27	26	27	1
50.0	18	18	18	18	19	18	0
100.0	11	12	11	11	11	11	0

* STD: Standard deviation

Plot 2: Average domain width (Figure 14)

A. Extrapolation Length = 1

h	Domain width $\overline{w}_d$					Average	STD
	128	256	384	512	640		
16	7.8	7.5	8	7.3	7.3	7.6	0.311448
32	8.9	8.1	9.2	8.8	9.2	8.8	0.450555
48	9.8	10.5	10.5	9.9	10.3	10.2	0.331662
64	11.9	11.8	12	12.5	11.9	12.0	0.277489
80	12.5	12.8	12.8	13.6	13.6	13.0	0.507937

96	14.5	14.8	15	15	15	15.1	0.238747

B. Extrapolation Length = 10

h	Domain width $\overline{w}_d$					Average	STD
	128	256	384	512	640		
16	10.5	9.5	10.5	10.5	10.5	10.3	0.447214
24	13.5	13.4	12.8	12.8	13	13.1	0.331662
32	14	13	14.5	15	15	14.2	0.83666
40	14	13.5	14.8	15	14.5	14.4	0.610737
48	16	15.8	16.8	16.8	17	16.5	0.54037
64	17	17.2	18	17.6	18	17.6	0.45607
80	17.3	18	18.5	18.5	19	18.3	0.642651
96	19.8	20.5	21	21	21	20.7	0.527257

C. Extrapolation Length = 20

h	Domain width $\overline{w}_d$					Average	STD
	128	256	384	512	640		
16	12	11.3	12.5	12.5	12.5	12.2	0.527257
20	13.3	13.2	13.3	13.3	13.4	13.3	0.070711
24	14.1	14.5	14.4	14.4	13.5	14.2	0.406202
28	15.5	15.2	15.5	15.8	14.8	15.2	0.374166
32	15.5	15.8	15.5	16.7	16.2	15.9	0.512835
36	16.6	16.9	17.1	16.8	16.8	16.8	0.181659
48	18.2	18.2	18.8	19	19.1	18.7	0.43359
64	19.7	21	20.5	20.5	20	20.3	0.502991
80	22.4	22.1	23.5	23.4	24	23.1	0.798123
96	25	26.1	24.5	25	25.5	25.2	0.605805

References

[1] M. J. Haun, *et al*, *Ferroelectrics*, **99**, 45 (1989)

[2] J. Junquera, P. Ghosez, *Nature*, **422**, 506 (2003)

[3] S. Nambu, D. Sagala, *Phys. Rev. B*, **50**, 5838 (1994)

[4] R. Kretschmer, K. Binder, *Phys. Rev. B*, **20**, 1065 (1979)

[5] Y. L. Li, L. E. Cross, L. Q. Chen, *J. Appl. Phys.* **98**, 064101 (2005)

[6] A. K. Soh, Y. C. Song, Y. Ni, *J. Am. Ceram. Soc.* **89**, 652 (2006)

[7] A. F. Devonshire, *Phil. Mag.* **40**, 1040 (1949)

[8] N. Ng, R. Ahluwalia, H. B. Su, F. Boey, *Acta Materialia*, **57**, 2047 (2009)

[9] C. L. Jia, et al, *Nature Mat* **6**, 64 (2007)

[10] F. Jona and G. Shirane, *Ferroelectric Crystals,* Dover (1961)

[11] W. Cao, *Ferroelectrics*, **375**, 28 (2008)

[12] S. Banerjee and P. Mukhopadhyay, *Phase Transformations*, Pergamon (2007)

[13] S. Nambu and D. A. Sagala, *Phys. Rev. B.* **50**, 5838 (1994)

[14] O. Axelsson and V. A. Barker, *Finite Element Solution of Boundary Value Problems: Theory and Computation***,** pp 64 – 100, SIAM (2001).

[15] Y. Ishibashi, H. Orihara, D. Tilley, *J. Phys. Soc. Jpn.* **67**, 3292 (1998)

[16] M. D. Glinchuk and A. N. Morozovskaya, *Phys. Stat. Sol. (B).* **238**, 81 (2003)

[17] L. Landau and E. Lifshits. *Statistical Physics I,* Pergamon, Oxford (1982)

[18] J. Schmelzer, *Nucleation theory and applications (1st ed),* Wiley-VCH (2005)

[19] W. Lu, et al, *Acta Mater,* **47**, 2913 (1999)

[20] V. C. Lo, *J. Appl. Phys.*, **94**, 3353 (2003)

[21] Z. X. Chen, Y. Chen and Y. S. Jiang, *J. Phys. Chem. B,* **105**, 5766 (2001); D. Vanderbilt, *Curr. Op. Sol. Stat. Mat. Sci*, **2**, 701 (1997)

[22] N. A. Pertsev, *et al*, *Phys. Rev. Lett.,* **80**, 1988 (1998).

[23] A. M. Bratvkovsky and A. P. Levanyuk, *Phys. Rev. Lett.,* **86**, 3642 (2001)

[24] D. A. Bonnell and S. V. Kalinin, *Mat. Res. Soc. Symp. Proc*.**688**, C9.5.1 (2002)

[25] T. Mitsui and J. Furuichi, *Phys. Rev.* **90**, 193 (1953)

[26] C. Kittel, *Phys. Rev.* **70**, 965 (1946)

[27] Y. G. Wang, W. L. Zhong and P. L. Zhang, *Phys. Rev. B.* **51**, 5311 (1995)

[28] S. K. Streffer, *Phys. Rev. Lett.,* **89**, 067601 (2002)

[29] G. Catalan, et al, *J. Phys: Condens. Matter.,* **19**, 022201 (2007)